Atomic Physics Division, Lund University

Master Thesis

Miniature Magnetic Quadrupole Lenses for a Laser-Plasma Accelerator

Lovisa Senje

June 16, 2011

Supervisor:
Olle Lundh

Abstract

In the past ten years, advances have been made in accelerating electrons with high-intensity lasers in laser-plasma accelerators. The electron beams from these accelerators demand other sorts of equipment than the ones from conventional accelerators, both because the pulse length of the electron beams is much shorter and because the scale of the accelerator is much smaller. An important piece of equipment is the magnetic quadrupole lens, which is used to focus and guide electron beams.

This master thesis project aimed to design, produce and characterize a set of miniature magnetic quadrupole lenses that can be used to control laser-plasma accelerated electron beams in a vacuum environment. The purpose of using miniature devices is to achieve focusing in the shortest possible distance after the source of the electrons and thereby preserve the short pulse length of the electron beams.

The characterization consisted of mapping the magnetic field strength inside the lenses and also determining the focal lengths of the lenses. Both simulations and experiments were carried out in order to perform this characterization. The experimental part of the project took place at the High Power Laser Facility at Lund University.

The magnetic field gradient inside the quadrupole lenses was measured to be in the region of 175 T/m. Comparing electron beams from the laser-plasma accelerator that had passed through a magnetic quadrupole lens with those that had not, the former were found to be less divergent. It was also possible to see that certain energies were focused more than others and thereby experimentally determine the energy-dependent focal length of the magnetic quadrupole lens.

Acknowledgements

My sincere thanks to everyone who has supported me throughout this master thesis project. Your help has been indispensable. I would especially like to thank the Ultra-High Intensity Laser Physics Group at the Atomic Physics Division for spending so much of their time helping me out with the laser and for in every way welcoming me into their group, Claes-Göran Wahlström for convincing me that physics is fascinating and my supervisor Olle Lundh for always finding time to support me, help me, critique my work, answer all my questions and never letting me feel that I disturb him.

Contents

Chapter 1

Introduction

1.1 Laser-Plasma Electron Acceleration

For a long time it has been possible to accelerate electrons in linear accelerators by using an oscillating electric field. These accelerators traditionally consists of metallic cavities and vary in length, depending on what final energy the electrons are supposed to reach, and can be up to several kilometres long. In 1979 Tajima and Dawson proposed that plasmas produced by high power lasers, could instead be used to accelerate the electrons [1]. The advantage would be that electrons could be accelerated to high energies over very short distances, since the lasers could create much stronger electric fields than regular linear accelerators. Tajima and Dawson's article was however of a theoretical nature and even though some advances were made over the years to put their theories into practice, it was not until 2004 that three independent research groups managed to produce high-quality, quasi-monoenergetic electron beams with lasers [2, 3, 4].

When a pulsed laser of sufficiently high power is focused in a gas, the first part of the pulse will turn the gas into a plasma, whilst the leading edge of the laser pulse displaces the electrons and excites oscillating electron plasma waves. The cause of this phenomenon is the ponderomotive force, which moves charged particles in strong electromagnetic fields. It pushes electrons away from regions with high intensity, such as the region inside the laser pulse, whereas heavier ions are less affected [5]. This separation of electrons from ions will create an electric field, which can accelerate charged particles. In order to actually achieve acceleration, electrons need to be injected into this field [6]. This is a task that is easier said than done, as the laser pulse propagates at the speed of light and the plasma wavelength is only $\sim$10-30 µm.

One way of achieving this sort of injection is to use wave breaking. The idea is that the individual electrons in the plasma wave reach the same velocity as the wave and can then end up being trapped and accelerated. Once these electrons have been accelerated the electron density in the plasma

wave is lowered and the wave is damped and the wave breaking stops [7]. Since the plasma wavelength is short, the pulse duration for the electron pulse in the beam can be extremely brief, even less than 10 fs.

In the experiments described in this thesis the electron beams typically have an energy of 100 MeV and a divergence of 5 mrad. The laser that is used to produce the electron beams has a pulse duration of approximately 40 fs and pulse energy of 1.7 J before compression and 1 J afterwards. This corresponds to a peak-power on the TW-scale. The gases that are used to produce the plasma are helium or hydrogen.

The possible areas in which laser-plasma accelerated electrons could be used, apart from being of interest as a physical phenomenon in themselves, are many. For example, in radiotherapy cancer treatments the patients are irradiated with X-rays, but research has shown that high energy electron beams, that could be produced with laser-plasma accelerators, are even more effective. Another example, is to let the electron beams hit solid targets of high atomic number and thereby convert the energy of the electrons into high-energy Bremsstrahlung photons, γ-rays. Due to the short pulse length of the electron beam and its small size, the γ-ray source will both be smaller and of shorter duration than conventional existing sources. These improved features could be used to better image how material compresses to high density, which is important in motor engineering and could also be used to inspect aircraft [8].

1.2 Steering and Manipulation of the Beam

Once a laser-plasma accelerated electron beam can be created, the next natural step would be to control the direction and divergence of the travelling electron beam. The most simple method to do this is perhaps to use a dipole magnet. Inside the magnet a homogeneous dipole field applies a force on the electrons which bends their paths. Although this method can be used to steer the electrons, it does not much affect the divergence of the beam. Even if an electron beam would have a seemingly small divergence, for example 5 mrad, the diameter of the beam after travelling 1 m would be increased by 5 mm. It would also bend the front of the pulse, as different electrons would have travelled different distances.

In optics divergent beams are a common phenomenon and there are many ways to control them, such as lenses and mirrors. Optical lenses and mirrors would however not focus an electron beam, but although other solutions need to be sought, the principle behind an optical lens might still be used.

When a beam of light passes from a material to another its path is bent a certain angle, depending on the materials and on the angle of incidence. Correspondingly, to bend the path of an electron beam a magnetic field could be applied, the stronger the field is the more the path of the electron

beam will be bent. A focusing optical lens is constructed in such a way that the further away from the center a ray hits the lens, the more its path will be bent from passing through the lens and therefore the beam will converge after the lens. If magnets could be arranged so that the further away from the optical axis an electron beam enters the magnetic field, the stronger it would be, then an equivalent of an optical lens could be built for electron beams.

A constellation of magnets that function as a lens for charged particles is a quadrupole magnet, see figure 2.1. These are used to focus electron beams in linear accelerators. Due to the size of these quadrupole lenses and the fact that they are electromagnets, they are unsuitable to use in a vacuum chamber. It is also highly desirable to maintain the short pulse length of the electron beam as it passes through the lens. This limits the possibilities of using the traditional quadrupole magnets, for laser-plasma accelerated electron beams and instead smaller devices with permanent magnets must be built. Such quadrupole magnets have been designed and discussed in various articles, for example references [9] and [10]. Some successful attempts have also been made to use this sort of permanent miniature quadrupole magnets for laser-plasma accelerated electron beams, that show that they are a suitable device to focus the beams [11].

1.3 Outline and Goal for Thesis

The aim of this thesis is to design, produce and test quadrupole magnets that are able to steer and focus electron beams produced with a laser-plasma accelerator. This is done both with simulations and with experiments.

The design of the quadrupole magnets is treated in chapter 2, along with simulations and characterization of their magnetic properties. Chapter 3 focuses on the use of the quadrupole lenses in a laser-plasma accelerator and includes simulations and results of experiments. In chapter 4 some conclusions are given based on the results from previous chapters and a short outlook for possible future projects is also included.

Throughout this thesis the term quadrupole is only referring to magnetic quadrupoles.

Chapter 2

Miniature Quadrupole Magnets

2.1 Quadrupole Magnets

When trying to focus and guide light an optical lens is used, but such a lens would rather clearly not be possible to use for electrons. Therefore it is necessary to resort to other techniques, when dealing with electron beams. A commonly used method is to make use of the Lorentz force, that is applied to electrons when they pass through a magnetic field. For electrons, in the absence of an electric field, this force is described by $\boldsymbol{F}_{\text{Lorentz}} = -e\,(\boldsymbol{v}_{\text{electron}} \times \boldsymbol{B})$. This means that the force is perpendicular to the direction of motion of the electrons, as well as to the magnetic field.

To focus an electron beam, a force that is pointed towards the center of the beam and that grows stronger towards the edges of the beam would be desirable. The magnetic field, and thereby also the force, should ideally increase linearly. Then the angle of bend, for electrons passing through the field, is proportional to the distance from the optical axis and the magnetic field will function as a focusing lens [12]. This can partly be achieved with the use of a quadrupole magnet. In their most simple form these consist of four magnets, as shown in figure 2.1. The magnetic fields from the four separate magnets cancel out completely in the center, but add together towards the edges and the strength of the field is proportional to the distance from the center.

If the direction of motion of the electrons is pointing into the paper then the Lorentz force has the direction as shown in figure 2.1. The electrons are then pushed in the direction of the force and as can be seen the quadrupole is focusing in one direction, whereas it is defocusing in a perpendicular direction. Consequently, at least two quadrupoles must be used if the aim is to achieve focusing in all directions at the same time.

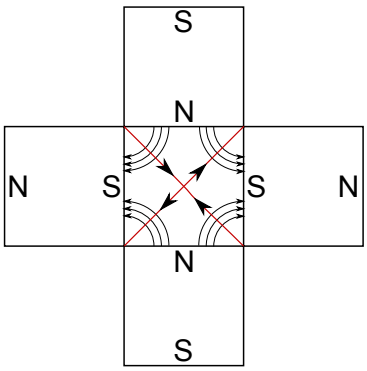

Figure 2.1: Quadrupole magnet, magnet field lines are marked in black and force field lines in red. It is assumed that the electron beam is travelling into the paper.

The focal length of a quadrupole depends on the gradient of the magnetic field inside the quadrupole, ∇B, the relativistic momentum of the particles passing through it, p, and also on its length, ω. The relativistic momentum is related to the energy of the electron, E, the mass of the electron, m_0, and the speed of light, c, through the relation $E^2 = (pc)^2 + \left(m_0 c^2\right)^2$. If the quadrupole is focusing along the x-axis and defocusing along the y-axis, the focal lengths can be expressed as

$$f_x = \frac{1}{k \cdot \sin(k \cdot \omega)} \quad , \quad f_y = -\frac{1}{k \cdot \sinh(k \cdot \omega)} \tag{2.1}$$

where, $k = \sqrt{\frac{\nabla B}{p/e}}$ [12]. This shows that the quadrupole lens will have different focal lengths for particles with different energies.

2.2 Design and Simulations of Quadrupole Lenses

2.2.1 Design Requirements

In order to design quadrupole lenses that are suitable to steer the electron beam from a laser plasma accelerator inside a vacuum chamber, it is necessary to achieve a high gradient of the magnetic field inside the quadrupole. The reason for this is to preserve the short pulse duration of the electron beam. The higher the gradient is the shorter distance will be needed to focus the beam, see equation 2.1, and the less difference in length there will be between the different electron paths from the quadrupole to the focus. The limited space available in the vacuum chamber also makes it important to have lenses with a short focal length and as can be seen in equation 2.1

this can be achieved by using a strong gradient. At the same time it is also important to ensure that the magnetic field outside the quadrupole is as low as possible, to minimize the impact of the quadrupole lens on other equipment in the vacuum chamber. These requirements can be achieved by letting the magnets be surrounded by an iron yoke, that also keeps the magnets in place. The thickness of the yoke is chosen in such a way that it is thick enough to insulate the surroundings from the magnets inside it and maximize the gradient of the magnetic field in the opening. However, it is also essential to keep the quadrupole magnet as light and small as possible.

2.2.2 Design

The magnets selected for the quadrupoles are principally made of neodymium, iron and boron and belong to the rare earth magnet family. These magnets are among the strongest permanent magnets available today. Two of the downsides of NdFeB magnets are that they shatter easily and that they are heat sensitive. The latter is a possible cause of concern if the laser beam continuously illuminates the magnet. To describe the strength of a NdFeB magnet a grading scale is used, which indicates the maximum energy product of the material the magnet is made from. This refers to the maximum strength the material can be magnetized to and is measured in units of MGOe (mega Gauss Oersted). The grading of the magnets in this project is N42, to be compared with the highest grading today which is N52.

The shapes of the four separate magnets, chosen to construct the quadrupole lenses, are rectangular cuboids. The front of the magnets, visible in figure 2.2, has the dimensions 6.4 mm x 6.4 mm (1/4" x 1/4"). These are then placed in an octagonal iron yoke, see figure 2.2, which is 8 mm thick. In between the magnets there are triangular wedges of aluminium to lend further support. Aluminium is chosen for its very low magnetic permeability. In the center there is another piece of aluminium with a cylindrical hole going through it with a 5 mm diameter, where the electron beam and laser beam will pass. The main purpose of this piece is to protect the fragile magnets from the diverging laser beam.

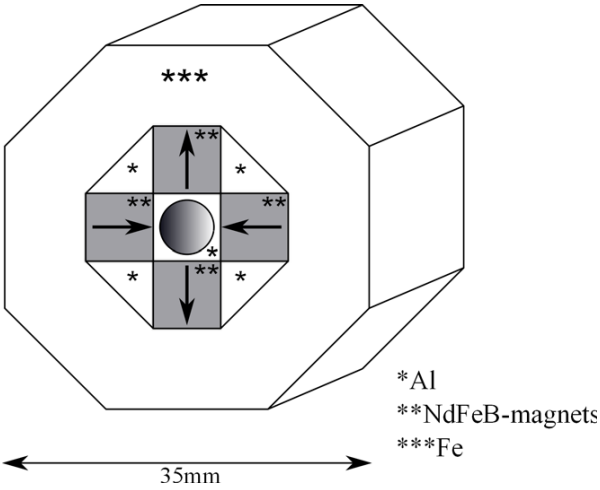

Figure 2.2: Complete quadrupole with yoke, the magnets are represented as grey, the iron and aluminium as white. The arrows indicate the direction of magnetization.

The quadrupole lenses are made in six different lengths, 6.4 mm (1/4”), 12.7 mm (1/2”), 19.1 mm (3/4”), 25.4 mm (1”), 31.8 mm (5/4”) and 50.8 mm (2”), in order to be able to focus electrons over a wide energy range. The finished quadrupole lenses can be seen in figure 2.3. The holes on the sides of the lenses are there to facilitate mounting the lenses inside the vacuum chamber.

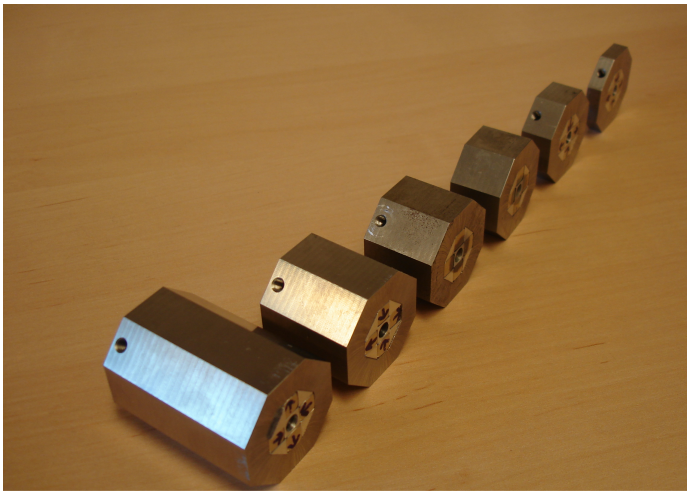

Figure 2.3: Mounted quadrupole magnets with yokes

2.2.3 Magnetic Field Simulations

To calculate the gradient of the magnetic field inside the quadrupole a simulation program called FEMM was used, which allows 2D simulations and is based on the finite element method. In figure 2.4 the flow and magnitude of the magnetic field in the quadrupole can be seen. In the center of the quadrupole lens the magnitude of the magnetic field is close to zero and it increases towards the edges, which means that one of the basic design requirements is fulfilled. Along the outside edges of the yoke the magnetic field is low, which was another of the design criteria.

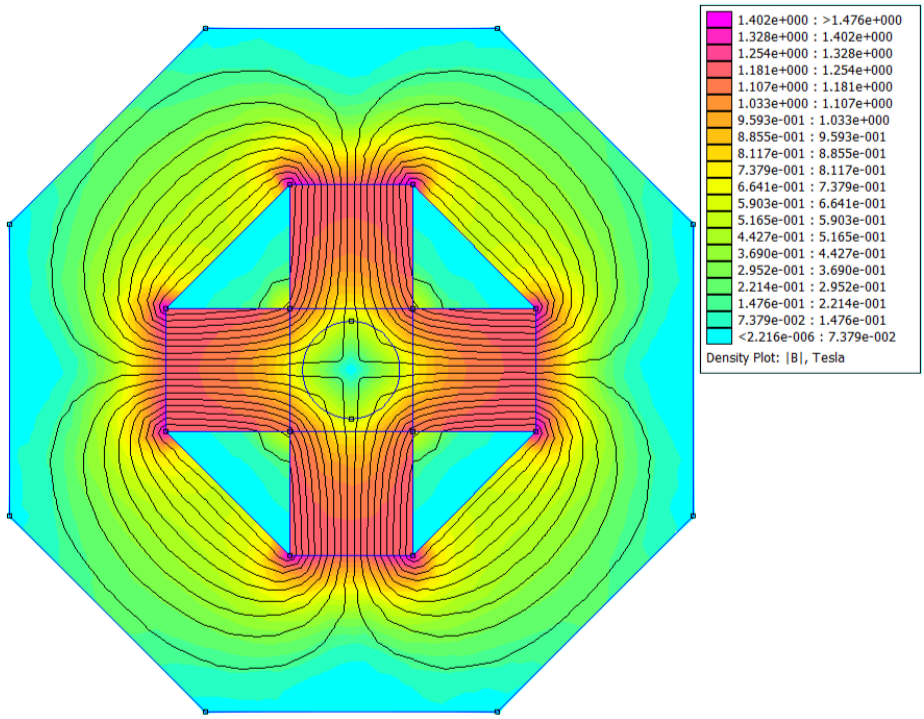

Figure 2.4: Illustration of the magnetic field in the quadrupole lens, as seen from the front.

From these simulations the magnetic field was calculated in 150 points across the diagonal of the opening. The component of the magnetic field which is perpendicular to the diagonal, $B_\perp$, is focusing or defocusing the electron beams whereas the tangential component, $B_\parallel$, ideally should be zero. The gradient of the magnetic field is therefore calculated from the simulated values of $B_\perp$. To understand how the design influences the gradient of the magnetic field, it is essential to study how ∇B depends on the size of the opening in the quadrupole lens. Figure 2.5 shows the importance of maintaining the opening as small as possible.

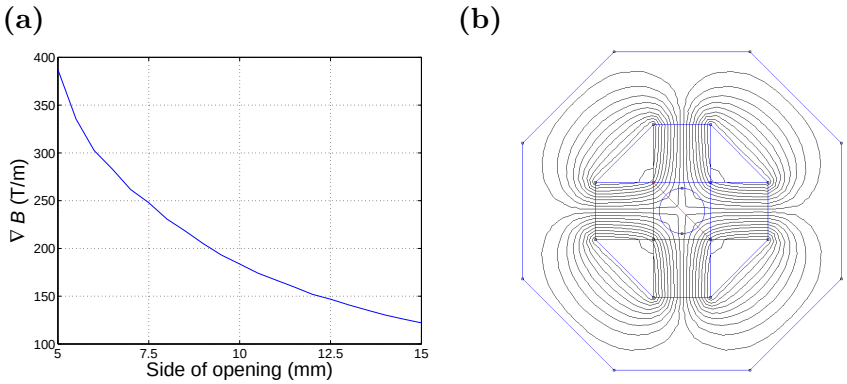

Figure 2.5: **(a)** ∇B as a function of the length of the sides in the quadratic opening of the quadrupole lens. **(b)** Front view of quadrupole with the diagonal along which the gradient was calculated marked in red.

In figure 2.6 the results from the simulations of the gradient in the quadrupole lenses, with parameters from the chosen design, are displayed. The magnetic field perpendicular to the diagonal, $B_{\perp\text{diag}}$, is plotted in figure 2.6 (a). A least square fit of a straight line was made to these values, marked as a red line in figure 2.6 (a), in order to calculate the gradient of the magnetic field.

It can be seen from the residual in figure 2.6 (b) that the gradient is not completely linear, especially towards the the corners of the opening. However, this should not affect the electrons that will pass through the central part. Figure 2.6 (c) shows that the component of the magnetic field that is tangential to the diagonal, $B_{\parallel\text{diag}}$ is very small. The gradient of the magnetic field is calculated to be 275 T/m.

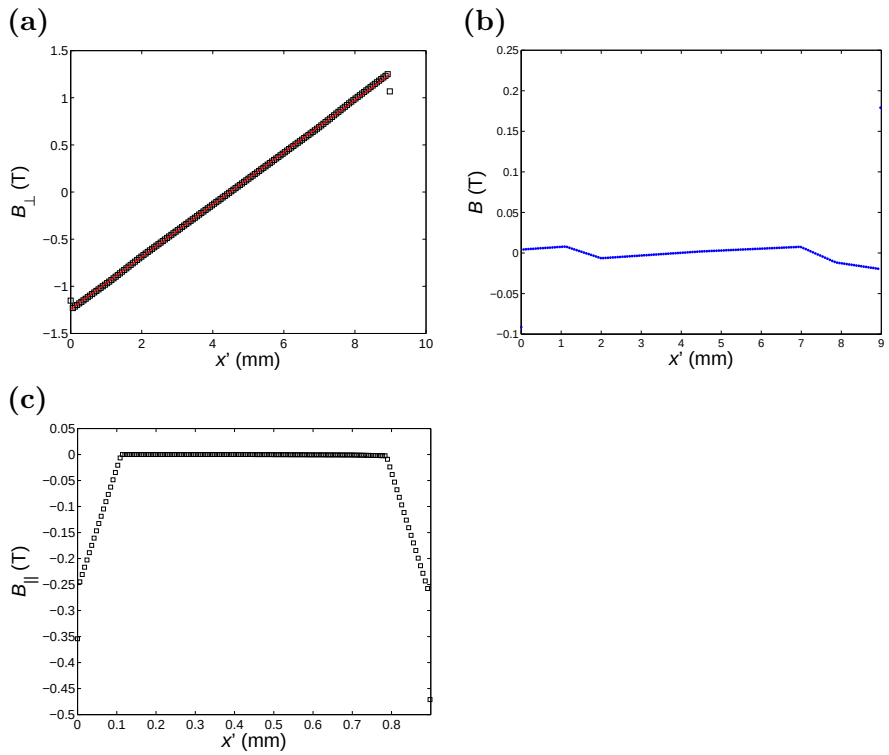

Figure 2.6: **(a)** The component of the simulated magnetic field normal to the diagonal with a linear fit in red. The x'-axis runs along the diagonal of the opening in the quadrupole lens and is marked in red in figure 2.5(b). **(b)** Residual between the simulated values and the linear fit. **(c)** The component of the simulated magnetic field tangential to the diagonal.

In table 2.1 the calculated focal lengths for 100 MeV electrons for the six different quadrupole lenses, according to equation 2.1, are given.

Length of Quadrupole Lens (mm)	Focal Length (mm)
6.4	191
12.7	98
19.1	67
25.4	52
31.8	31
50.8	13

Table 2.1: The focal lengths for different quadrupole lenses where ∇B is 275 T/m and the energy of the electrons is 100 MeV.

The simulations carried out in this section indicate that the design chosen for the quadrupole lenses is appropriate and that they have a gradient which is strong enough to focus electron beams produced with a laser-plasma accelerator, such as the one at the High Power Laser Facility at Lund University.

2.3 Matrix Formulation

A system of quadrupole magnets can be described with a matrix formulation similar to the one used for ordinary optical systems. The basic principle is that if a set of n components have transport matrices $\boldsymbol{A_1}, \boldsymbol{A_2}, ..., \boldsymbol{A_n}$ and the initial position along the x-axis (perpendicular to the axis of propagation), x_i, as well as the angle of incidence, θ_i are known, then the position, x_f, and angle, θ_f, can be calculated at the end of the system through the relation

$$\begin{pmatrix} x_\mathrm{f} \\ \theta_\mathrm{f} \end{pmatrix} = \boldsymbol{A_n} \cdot \boldsymbol{A_{n-1}} \cdot ... \cdot \boldsymbol{A_1} \begin{pmatrix} x_\mathrm{i} \\ \theta_\mathrm{i} \end{pmatrix} \tag{2.2}$$

For a thin lens the transport matrix is

$$\boldsymbol{A_{lens}} = \begin{pmatrix} 1 & 0 \\ -\dfrac{1}{f} & 1 \end{pmatrix} \tag{2.3}$$

where f is the focal length of the lens. The corresponding matrix for a thin quadrupole lens looks exactly alike[12]. However, the focal length is not the same in all directions, see equation 2.1, and it is therefore important to define in which direction the matrix is valid, as $\boldsymbol{A_{lens\ x}} \neq \boldsymbol{A_{lens\ y}}$.

$$\boldsymbol{A_{lens\ x}} = \begin{pmatrix} 1 & 0 \\ -\dfrac{1}{f_\mathrm{x}} & 1 \end{pmatrix} \quad , \quad \boldsymbol{A_{lens\ y}} = \begin{pmatrix} 1 & 0 \\ -\dfrac{1}{f_\mathrm{y}} & 1 \end{pmatrix} \tag{2.4}$$

Another important transport matrix required in order to describe a system of quadrupole lenses, is the matrix representing drift space. A drift of a distance, l, is represented in the matrix formulation by

$$\boldsymbol{A_{drift}} = \begin{pmatrix} 1 & l \\ 0 & 1 \end{pmatrix} \tag{2.5}$$

However, all quadrupole lenses do not have a negligible thickness. The matrix representation of a such a lens, with thickness ω and focal length f, can be approximated by using the matrices of two drift spaces and that of a thin lens [14] as shown in equation 2.6

$$\boldsymbol{A_{thick\ lens}} = \begin{pmatrix} 1 & \frac{\omega}{2} \\ 0 & 1 \end{pmatrix} \begin{pmatrix} 1 & 0 \\ -\frac{1}{f} & 1 \end{pmatrix} \begin{pmatrix} 1 & \frac{\omega}{2} \\ 0 & 1 \end{pmatrix} \tag{2.6}$$

For a more thorough treatment of matrix formulation see reference [15].

2.4 Matrix Calculations

A system of two quadrupole lenses can be used to make a divergent beam parallel. These lenses need to be placed in a correct position that can be calculated from a matrix formulation of the system. The distance from the source of the particles to the first quadrupole is denoted l_1 and the distance between the two quadrupoles l_2. If the lenses are assumed to be thin, then the matrix formulation of the problem becomes

$$\begin{pmatrix} x_\mathrm{f} \\ \theta_\mathrm{f} \end{pmatrix} = \underbrace{\begin{pmatrix} 1 & 0 \\ -\frac{1}{f_2} & 1 \end{pmatrix} \begin{pmatrix} 1 & l_2 \\ 0 & 1 \end{pmatrix} \begin{pmatrix} 1 & 0 \\ -\frac{1}{f_1} & 1 \end{pmatrix} \begin{pmatrix} 1 & l_1 \\ 0 & 1 \end{pmatrix}}_{\boldsymbol{A_{\mathrm{tot}}}} \begin{pmatrix} x_\mathrm{i} \\ \theta_\mathrm{i} \end{pmatrix} \tag{2.7}$$

By simply using matrix multiplication an expression for $\boldsymbol{A_{\mathrm{tot}}}$ can be derived

$$\boldsymbol{A_{\mathrm{tot}}} = \begin{pmatrix} 1 - \dfrac{l_2}{f_1} & l_1 + l_2\left(\dfrac{l_1}{f_1}\right) \\ -\dfrac{1}{f_2} - \dfrac{1}{f_1}\left(1 - \dfrac{l_2}{f_2}\right) & -\dfrac{l_1}{f_2} + \left(1 - \dfrac{l_2}{f_2}\right)\left(1 - \dfrac{l_1}{f_1}\right) \end{pmatrix} \tag{2.8}$$

As the beam should become parallel, θ_f must be equal to zero regardless of the initial value for θ_i. When the particles come from a point source, $x_i = 0$, it is possible to see from

$$\begin{pmatrix} x_f \\ 0 \end{pmatrix} = \boldsymbol{A_{\mathrm{tot}}} \begin{pmatrix} 0 \\ \theta_i \end{pmatrix} \tag{2.9}$$

that a necessary condition for a parallel output is that

$$-\frac{l_1}{f_2} + \left(1 - \frac{l_2}{f_2}\right)\left(1 - \frac{l_1}{f_1}\right) = 0 \tag{2.10}$$

Since the lenses are assumed to be thin $f_x \approx -f_y$, as $\sin a \approx \sinh a$ for small a, see equation 2.1. Equation (2.10) must be fulfilled in both in the x- and y-directions, which leads to the following systems of equations:

$$\begin{cases} -\dfrac{l_1}{f_2} + \left(1 - \dfrac{l_2}{f_2}\right)\left(1 - \dfrac{l_1}{f_1}\right) = 0 \\ \dfrac{l_1}{f_2} + \left(1 + \dfrac{l_2}{f_2}\right)\left(1 + \dfrac{l_1}{f_1}\right) = 0 \end{cases}$$

$$\Longleftrightarrow$$

$$\begin{cases} 1 - l_1\left(\dfrac{1}{f_1} + \dfrac{1}{f_2}\right) - \dfrac{l_2}{f_2} + \dfrac{l_1 l_2}{f_1 f_2} = 0 \\ 1 + l_1\left(\dfrac{1}{f_1} + \dfrac{1}{f_2}\right) + \dfrac{l_2}{f_2} + \dfrac{l_1 l_2}{f_1 f_2} = 0 \end{cases}$$

$$\Longleftrightarrow$$

$$\begin{cases} f_1 f_2 + l_1 l_2 = 0 \\ l_1 (f_1 + f_2) + f_1 l_2 = 0 \end{cases} \tag{2.11}$$

From this equation it can then be concluded that to achieve a parallel beam with two thin quadrupole lenses the lenses must be positioned according to

$$l_1 = \sqrt{\frac{f_1}{\frac{1}{f_1} + \frac{1}{f_2}}} \quad l_2 = \sqrt{f_2 (f_1 + f_2)} \tag{2.12}$$

It should be noted that a conclusion from equation 2.12 is that $f_1 \neq -f_2$, which motivates the design of quadrupole lenses of different lengths. What is also important to bear in mind is that although the beam is parallel, it is deformed, i.e. $x_\mathrm{f} \neq y_\mathrm{f}$. In order to produce circular parallel beams more than two quadrupoles need to be used.

With similar methods the correct lens positions for other sorts of focusing, such as point to point, can be calculated.

In this master project the use of one quadrupole at the time has been the main focus, but the above calculations are important in the design of the quadrupole magnets so that they can be used in future experiments.

2.5 Measurements

An important part of characterizing the quadrupole lenses is to measure the magnetic field inside the opening where the electrons will pass. This can be done using a hall probe connected to a Gaussmeter. The opening in the quadrupole is only a few millimetres wide which makes it necessary to use a thin hall probe in order to accurately measure the magnetic field close to the corners.

A transverse Hall probe, approximately 1 mm wide, was mounted on translation stages in such a way that motors could control its motion in 3D, as seen in figure 2.7. A script was written in LabView to steer the translation stages and thereby also the position of the probe, according to a map of coordinates and to collect the data from the Gaussmeter.

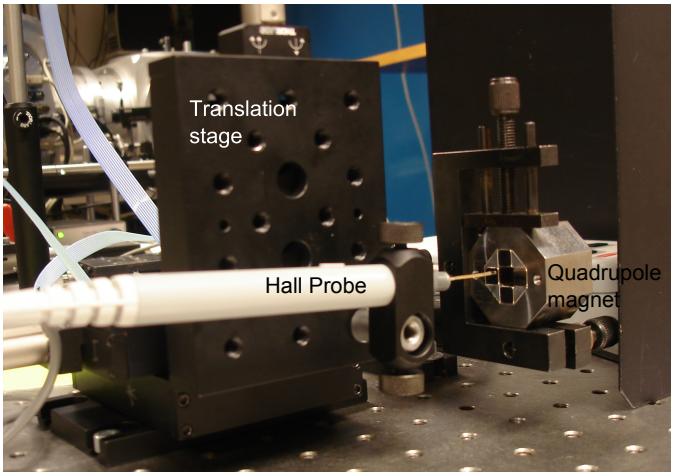

Figure 2.7: The setup for measuring the magnetic field inside the quadrupole

The central piece of aluminium with the cylindrical hole through it, see figure 2.2, was removed to facilitate the scan. In the measurement, data was recorded from 1024 points across a 6.1 mm x 6.1 mm area, halfway through the length of the quadrupole lens. First the probe was oriented to measure the vertical field and then the probe was rotated 90 degrees to measure the horizontal field in the same measurement points. Thereafter the magnitude of the magnetic field was calculated. Figure 2.8(a) shows the magnitude of the magnetic field in a plane inside the quadrupole.

It is also interesting to see how the field lines of the magnetic field runs inside the quadrupole lens. Figure 2.8(b) demonstrates that the measured field lines are similar to those in figure 2.1 (although the poles a rotated 90 degrees) and the simulated ones in figure 2.4.

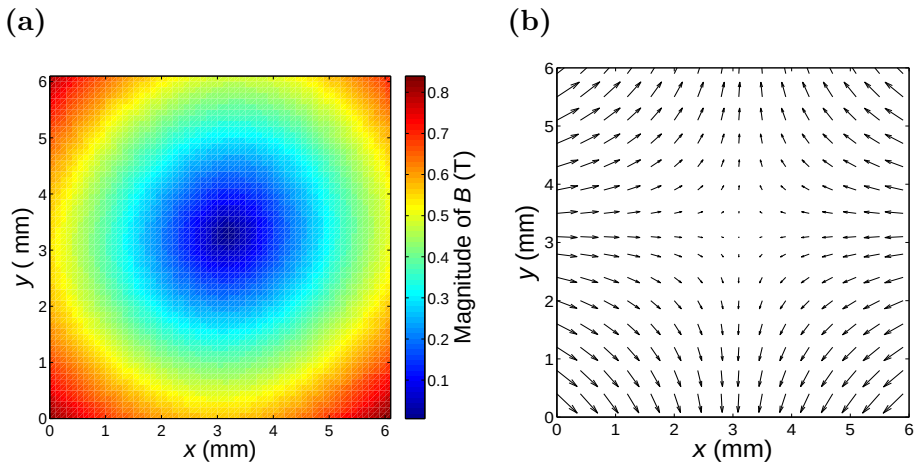

Figure 2.8: **(a)** The magnitude of the magnetic field in a vertical plane halfway through the quadrupole magnet with length 25.4 mm. **(b)** A vector plot of the magnetic field from (a).

The gradient of the field can be generated from the data across the diagonal of the quadrupole, compare with figure 2.6. The same method was used as in section 2.2.3, i.e. by fitting the data with the least square method with a straight line. Then the constant derivative of the line will be the gradient of the magnetic field. In figure 2.9 the measured values of the component of the magnetic field normal to the diagonal, $B_\perp$, as well as the fit and the residual are shown.

The value of ∇B varies depending on how far towards the corners of the quadrupole the values are included in the fit. For the conditions in figure 2.9 the gradient is 172 T/m, around 55% lower than the simulated value. Equivalent measurements and calculations has also been performed with the 19.1 mm long quadrupole magnet and the gradient was 175 T/m. A reason for these lower values could be that the simulations were made in an 2D-environment and the quadrupole was there assumed to have an infinite length, whereas in reality this is obviously not the case. Another possible cause is that the corners of the four actual NdFeB magnets are rounded, unlike in the simulations, making the opening slightly larger. Yet another possible cause is that the inside of the yokes have not been polished and thus the contact surface between the magnets and the yoke is smaller. The strength of the free NdFeB-magnets on the surface (0.4 T) is confirmed to be the same as in the simulation program ($\pm 5\%$).

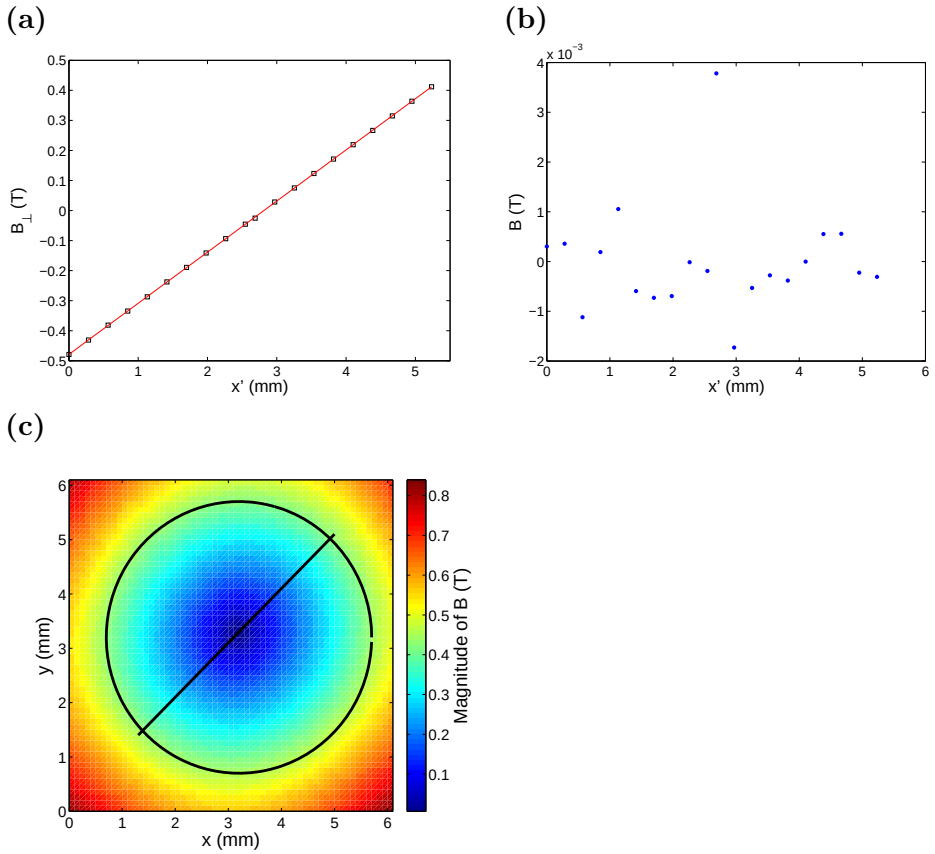

Figure 2.9: **(a)** The measured values of $B_\perp$ and the linear fit. x' is the axis marked with a black straight line in (c). **(b)** The residual between the linear fit and the measured values from (a). x' is the axis marked with a black straight line in (c). **(c)** The x'-axis and the position of circular opening in the protective piece of aluminium, see section 2.2.2, marked in black in a magnitude plot of B. The length of the quadrupole magnet is 25.4 mm.

From the residual it is possible to draw the conclusion that the measurements of gradient are showing an almost completely linear behaviour. This indicates that the field will function well as a lens and that it is possible to focus electron beams.

The technique to rotate the probe gives a certain inaccuracy to the measurements, as they will only be precise if the two sets of measurements are carried out in exactly the same points. The grid of the measurement points is very fine (approximately 200 µm between each measurement) and it is difficult to manually align the probe after the rotation with such precision and therefore this gives a limit for the accuracy of the data.

What also needs to be considered is how the magnetic field varies towards the edges of the quadrupole magnet and just outside it. The data displayed

in figure 2.10 is taken from 14 mm into the 24.5 mm long lens to 6 mm outside. What has been measured is both the horizontal and the vertical components of the magnetic field, B_{x} and B_{y}, in 100 points along the z-axis. Figure 2.10 demonstrates how the magnitude, $B_{\mathrm{mag}} = \sqrt{B_{\mathrm{x}}^2 + B_{\mathrm{y}}^2}$, of the magnetic field declines. The longitudinal component of the magnetic field, B_{z}, is assumed to be negligibly small.

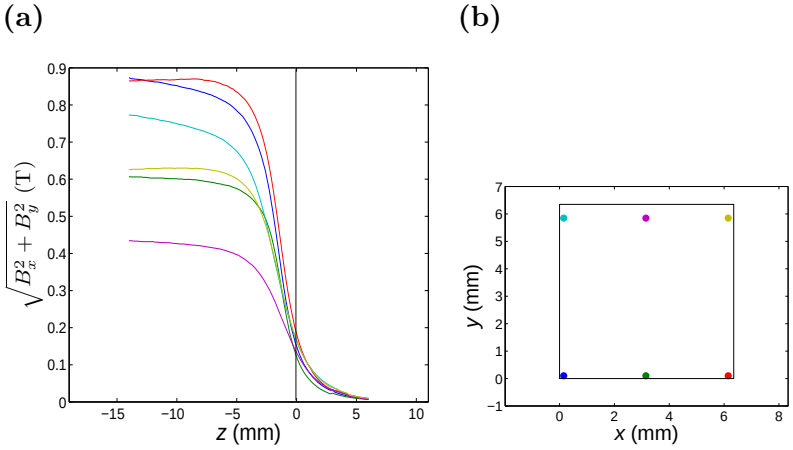

Figure 2.10: **(a)** The horizontal and vertical fringe field recorded along the z-axis from 14 mm inside the 25.4 mm long quadrupole magnet to 6 mm outside at six different xy-positions marked in (b). The edge of the quadrupole is marked with a black line. **(b)** The positions from (a) marked with their colors in a cross section of the opening.

The fact that there is not a perfect step in the magnetic field at the edge of the quadrupole lens means that the effective length of the quadrupole lens will be different than its physical length. The relation between the physical and the effective lengths of the quadrupole is given by equation 2.13, where ω_{eff} is the effective length of the quadrupole, $G(z)$ is the magnetic field and G_0 denotes the constant interior quadrupole strength [13].

$$\omega_{\mathrm{eff}} = \frac{1}{G_0} \int_{-\infty}^{\infty} G(z) \mathrm{d}z \tag{2.13}$$

An averaged numerical integration of the six different plots in figure 2.10 reveals that the effective length of the quadrupole lens is approximately 2 mm shorter than its physical length. The fringe fields for the other quadrupole lenses have not been measured, but are assumed to be similar. For the shortest of the quadrupole lenses, ω=6.4 mm and ω=12.7 mm, this will affect the focal length, but for the longest lenses the effect will be more negligible, as $\omega >> 2$ mm. For example, the focal length for a 25.4 mm long

quadrupole lens with ∇B=172 T/m, is changed from 80 mm to 85 mm for electrons of 100 MeV. In figure 2.10 it can also be seen that the magnetic field declines rapidly around the edge of the quadrupole lenses.

The fact that the measured gradient is so much lower than expected from the simulations, will affect the focal lengths of the quadrupole lenses, see equation 2.1 and table 2.2. This can cause problems in maintaining the short pulse duration of the electron beam.

Energy (MeV)	Focal Length (mm) ∇B=275 T/m ω=25.4 mm	Focal Length (mm) ∇B=172 T/m ω_{eff}=23.4 mm
50	29	46
60	33	54
70	38	62
80	43	70
90	48	79
100	52	87

Table 2.2: A comparison between the focal lengths of the 25.4 mm long quadrupole lens, with the simulated and measured parameters, for different energies.

Chapter 3

Experiments with Quadrupole Lenses

3.1 Experimental Method

It is important to understand what energy that is focused by the quadrupole lens at a certain distance. With such knowledge the properties of the quadrupole magnet can be characterized and it is thereby possible to use it to improve precision in other experiments.

In order to be able to determine the focal length of the quadrupole lenses a dipole magnet is used. By letting the electrons pass through a homogeneous dipole field their paths will be bent along a circular arc. The radius of curvature for this arc, the Larmor radius, depends on the relativistic momentum of the electrons, p, the strength of the dipole magnet, B_{dipole}, and the charge of the electrons, $q(=\text{-}e)$, according to equation 3.1. This means that electrons of different energies will be separated and it is thus possible to identify electrons of a specific energy.

$$R = \frac{p}{|q|B} \tag{3.1}$$

The experimental setup is shown in figure 3.1. A laser is focused by a curved mirror into the gas jet, the source of the electrons. There the electrons are accelerated and then travel through the magnetic quadrupole lens. After passing through the dipole and drifting a short distance the electron beam hits a screen. Where the screen is hit by electrons, it emits light of a strength that is proportional to the number of electrons. The screen is then imaged by a camera. The more electrons that hit a certain spot on the screen, the brighter the corresponding spot will be on the image. In the experiments performed in this master project, the electron beams had a continuous energy spectrum.

By placing a quadrupole lens and a magnetic dipole in the path of the electron beam, the focal length of the lens can be determined. First the

quadrupole will focus electrons of one energy in the beam and then the dipole will separate the energies and it can be decided which energy is actually being focused.

The method used in the experiments was to position the quadrupole lens and the dipole magnet in such a way that the dipole separates the energies in a perpendicular direction of the one the quadrupole focuses in. The purpose of this approach is that the positions where the electrons hit the screen will form an hourglass shape, with the position of the waist corresponding to the focused energy.

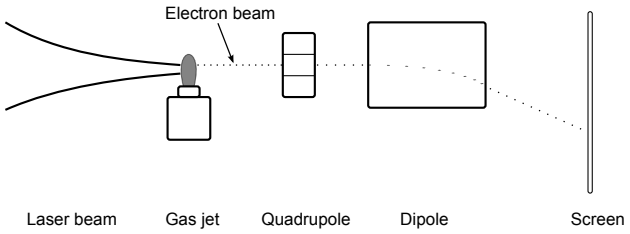

Figure 3.1: The path of a monoenergetic electron beam from source to screen

In figure 3.2 a photograph from inside the vacuum chamber can be seen. The dipole magnet was not in place when the photograph was taken.

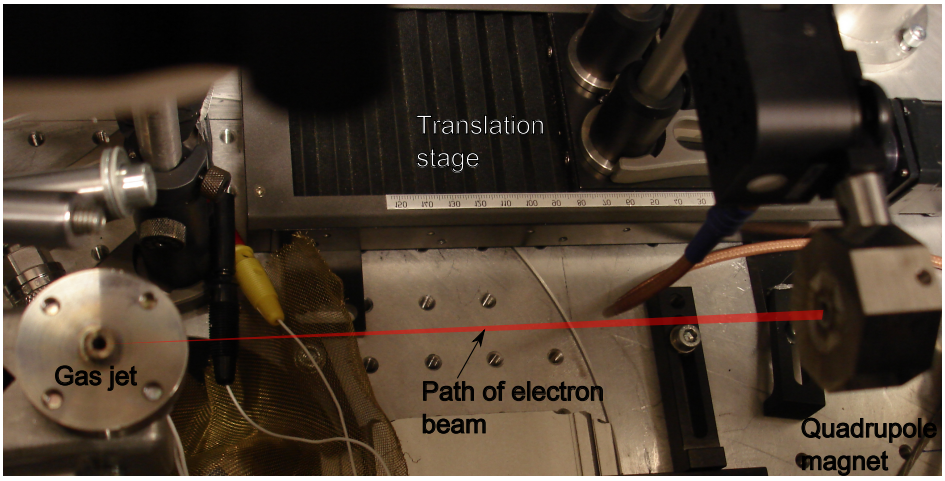

Figure 3.2: A photo of the mounted quadrupole magnet inside the chamber

3.2 Matrix Formulation of the Experimental Setup

The electron beam passes through the setup illustrated in figure 3.1. This system can be represented with matrices and these can be used to calculate where an electron with a specific energy and with an initial angle between the direction of motion and the optical axis, denoted θ_i, will hit the screen. The matrix representation will be different in the x- and y-directions since the quadrupole is focusing in one direction and defocusing in the other and the dipole magnet will only bend the path of the electrons in one direction.

It is assumed that the quadrupole lens is focusing in the x-direction and that the magnetic field from the dipole magnet separates the energies of the electrons in the y-direction. The dipole is assumed to be ideal, i.e. with a homogeneous field inside the magnet and completely without any fringe fields. Any focusing effects of the fringe field of the dipole are thus ignored. The length of the quadrupole is denoted ω, the length of the dipole a and the drift spaces with dr_n.

$$\boldsymbol{A}_{\mathbf{tot\ x}} = \begin{pmatrix} 1 & dr_3 \\ 0 & 1 \end{pmatrix} \underbrace{\begin{pmatrix} 1 & a \\ 0 & 1 \end{pmatrix}}_{\text{Dipole}} \begin{pmatrix} 1 & dr_2 \\ 0 & 1 \end{pmatrix} \underbrace{\begin{pmatrix} 1 & \frac{\omega}{2} \\ 0 & 1 \end{pmatrix} \begin{pmatrix} 1 & 0 \\ -\frac{1}{f_x} & 1 \end{pmatrix} \begin{pmatrix} 1 & \frac{\omega}{2} \\ 0 & 1 \end{pmatrix}}_{\text{Quadrupole}} \begin{pmatrix} 1 & dr_1 \\ 0 & 1 \end{pmatrix} \tag{3.2}$$

Note that the matrix representing the dipole in the x-direction is equivalent to that of a drift space. The matrix representation in the y-direction is made in a similar way, but the dipole magnet and the last drift space is treated analytically. The vertical displacement, d, from where the electrons enter the dipole magnet until they hit the screen is

$$d = \sqrt{R^2 - \hat{x}^2} - \sqrt{R^2 - (a - \hat{x})^2} + dr_3 \frac{a - \hat{x}}{\sqrt{R^2 - (a - \hat{x})^2}}, \tag{3.3}$$

$$\text{where } \hat{x} = \frac{R \tan\theta}{\sqrt{1 + \tan^2\theta}}$$

R is the Larmor radius, see equation 3.1, and θ is the angle of incidence of the electrons, where $\theta = 0$ indicates that the electrons travel along the optical axis. For more detailed derivation of how the dipole displaces electrons vertically see appendix A.

3.3 Monte-Carlo Simulations

To be able to predict and afterwards also analyse the electron spectra that would appear on the screen in figure 3.1, simulations based on the matrix formulation of the experimental setup were made. The aim was to investigate whether there would be a visible waist of the spectra for the energy that is focused by the quadrupole.

The simulations were done with the Monte-Carlo method. The principle behind this method is to give slightly different initial conditions to a large quantity of electrons and then follow the path of each individual electron from the source through the system and determine where it hits the screen. The final positions of all the electrons make up a simulated image of the one the camera would take of the screen in the experiments. Although it is, strictly speaking, not completely the correct terminology, this image will from here on be referred to as an energy spectrum.

In order to perform these simulations MATLAB was used for the numerical calculations. Every simulation included one million electrons. Each electron was given two separate initial angles, $\theta_{\mathrm{i\ x}}$ and $\theta_{\mathrm{i\ y}}$, from a Gaussian distribution, two initial coordinates, x_{i} and y_{i}, from a Gaussian distribution and an energy from a uniform distribution. θ represents the angle between the direction of motion and the optical axis. It is assumed that the electrons come from a point source in the longitudinal direction, i.e. $z_{\mathrm{i}} = 0$.

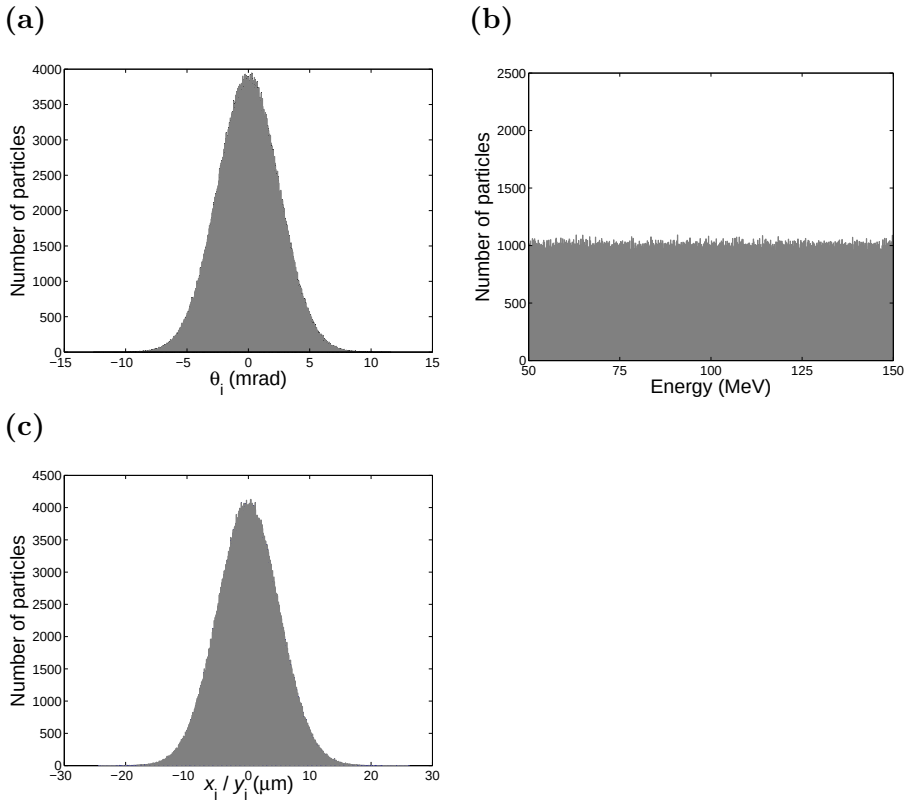

Figure 3.3: Histogram with 1000 bins of the initial distributions of one million electrons of **(a)** angle of incidence in one directions (x or y), **(b)** the energy of the electrons, **(c)** the initial x- or y-coordinate.

Figure 3.3 demonstrates the distributions, which were chosen to reflect the electron beams produced at the High Power Laser Facility at Lund University, i.e. the angle of divergence is ∼5 mrad (FWHM), the distribution of the initial position is 10 µm (FWHM) and the energy is centred around 100 MeV.

The matrices in the two directions from section 3.2 were then multiplied with the matrices with initial conditions for each electron, like in equation 2.2.

$$\begin{pmatrix} x_\mathrm{f} \\ \theta_\mathrm{f} \end{pmatrix} = \boldsymbol{A}_{\mathbf{tot\ x}} \begin{pmatrix} x_\mathrm{i} \\ \theta_\mathrm{i} \end{pmatrix} \quad , \quad \begin{pmatrix} y_\mathrm{f} \\ \theta_\mathrm{f} \end{pmatrix} = \boldsymbol{A}_{\mathbf{tot\ y}} \begin{pmatrix} y_\mathrm{i} \\ \theta_\mathrm{i} \end{pmatrix} \tag{3.4}$$

Finally a summary was made of where these simulated electrons hit the screen, x_f and y_f, and this was represented in a histogram as the energy spectrum. Figure 3.4 shows that it is possible to find a position for the quadrupole so that the spectrum has a waist, corresponding to the energy focused by the quadrupole lens.

The focal length of the quadrupole lens is depending on the energy of the electron, see equation 2.1. If the distance from the source to the quadrupole changes, so will the energy that is focused. To investigate whether this effect would be visible on the electron spectra, simulations where this distance was varied were made. In figure 3.4 it is clearly visible that the closer the quadrupole is to the source, the lower energy is focused. The position of the quadrupole and the dipole magnet with respect to the source and the screen, were chosen to reflect the conditions in the experiments.

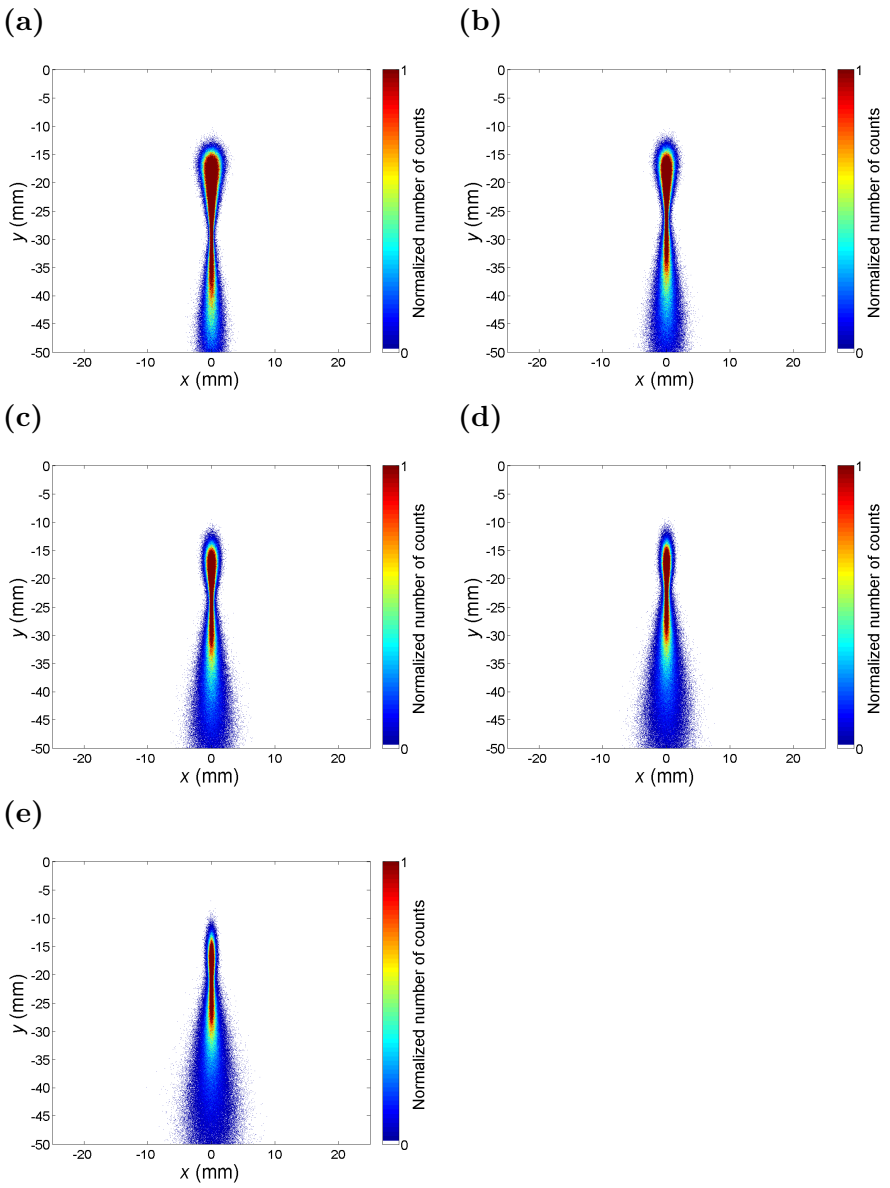

Figure 3.4: Energy spectra where the distance from the source to the front edge of the quadrupole is varied. y=0 is the optical axis, i.e. $E_{\text{electron}} = \infty$ corresponds to y=0. The colour scale represents the concentration of electrons hitting the screen in a certain point. The quadrupole magnet is 19.1 mm long, the dipole magnet 50 mm, ∇B=275 T/m and B_{dipole}=0.7 T. The distance from the back of the dipole to the screen is 204 mm and the total distance from the source to the screen is 387 mm. The distance between the gas jet and the quadrupole is **(a)** 58 mm **(b)** 68 mm **(c)** 78 mm **(d)** 88 mm **(e)** 98 mm.

What happens if the center of the electron beam does not coincide with the center of the quadrupole lens? In figure 3.5 the center of the electron beam was given a small offset, 0.5 mm, in the horizontal direction and as a result the whole spectrum is tilted around the waist of the spectrum. The larger the offset is, the larger is the tilt.

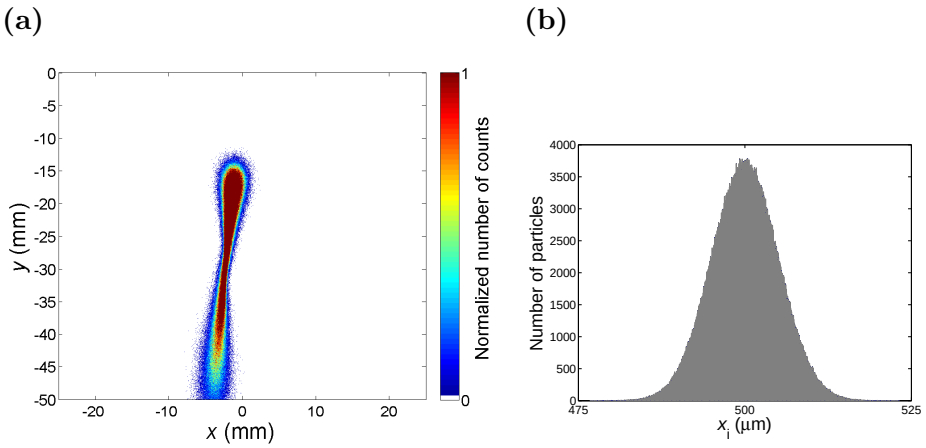

Figure 3.5: **(a)** A simulated energy spectrum with 0.5 mm offset in x_i. The quadrupole magnet is 19.1 mm long, ∇B=275 T/m, B_{dipole}=0.7 T and the distance from the source to the front of the lens is 58 mm. **(b)** Histogram with 1000 bins of the initial distribution of x_{i} with 0.5 mm offset.

In the experiments the offset might be caused by a misalignment in the setup or by fluctuations from shot to shot in the electron beam. The tilt is caused by the different focal lengths of the quadrupole for different energies. The electrons of the energy that is in focus are not affected, since the quadrupole will steer these to the optical axis, which is considered to pass through the center of the quadrupole lens, exactly at the screen. However, the quadrupole will overcompensate the displacement for electrons with too low energy and they will consequently hit the screen to the side of the optical axis. For electrons with higher energy than the one in focus, the quadrupole lens will undercompensate for the horizontal displacement and they will thus hit the screen on the other side of the optical axis.

An offset for the center of the electron beam in the vertical direction will not cause any such obvious changes to the spectrum, which can also be verified by comparing figure 3.6(a) with 3.4(a). The only parameter that differs in the two spectra is the vertical offset. The reason is that the quadrupole lens is already defocusing in this direction.

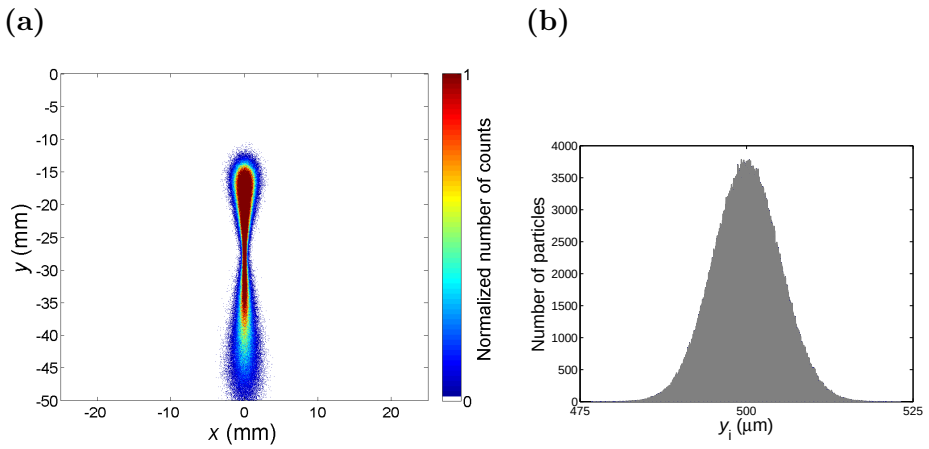

Figure 3.6: **(a)** A simulated energy spectrum with 0.5 mm offset in y_i. The quadrupole magnet is 19.1 mm long, ∇B=275 T/m, B_dipole=0.7 T and the distance from the source to the front of the lens is 58 mm. **(b)** Histogram with 1000 bins of the initial distribution of y_i with 0.5 mm offset.

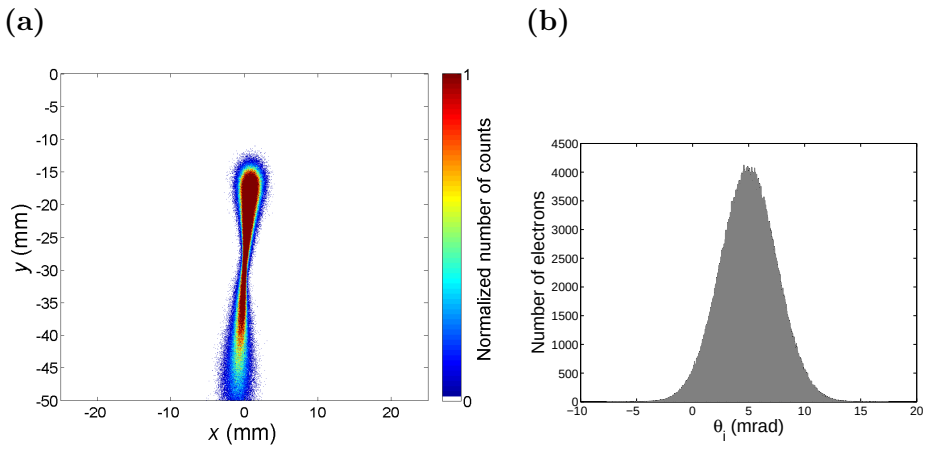

Figure 3.7: **(a)** A simulated energy spectrum with 5 mrad offset in θ_i. The quadrupole magnet is 19.1 mm long, ∇B=275 T/m, B_dipole=0.7 T and the distance from the source to the front of the lens is 57.8 mm. **(b)** Distribution of θ_i with 5 mrad offset for 1 million particles.

Another possibility is that there is an offset in the initial angle between the direction of motion for the electrons and the optical axis, θ_i. As can be seen from figure 3.7 this will give a similar spectrum to the offset in the horizontal direction. The principle behind it is the same, since having an offset in θ_i will cause the center of the beam to pass through the quadrupole with an offset from the optical axis.

It is also interesting to investigate how the angle of the spectrum increases with an offset. Figure 3.8 displays this relationship and shows the importance of having a stable beam that does not fluctuate from shot to shot. Even a small fluctuation of a few mrad between the electron beam and the lens, will cause a very noticeable angle in the spectrum.

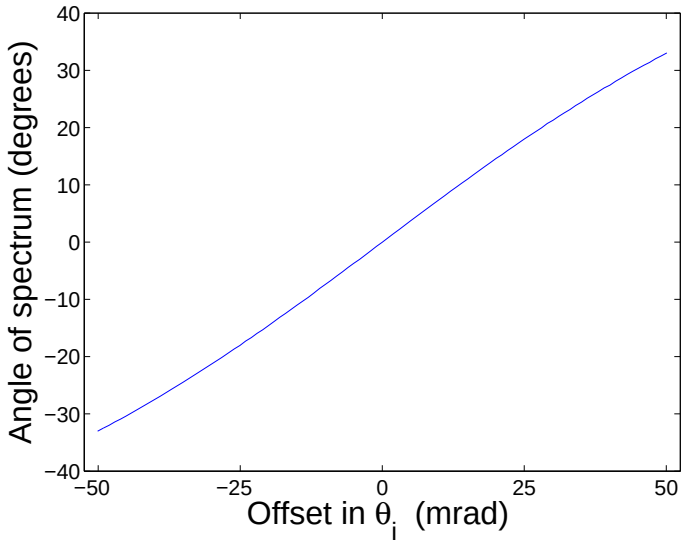

Figure 3.8: Simulation of the correlation between θ_{i} and the angle of the spectrum. The length of the quadrupole lens is set to 25.4 mm and the distance between the source and the lens to 57.8 mm.

3.4 Simulations of Beam Envelope

With a simulation program called TraceWin it is possible to illustrate the envelope of the electron beam. In figure 3.9 three different envelopes are displayed, one shows an electron beam that is focused before the screen, one on the screen and the third one would have been focused after the screen.

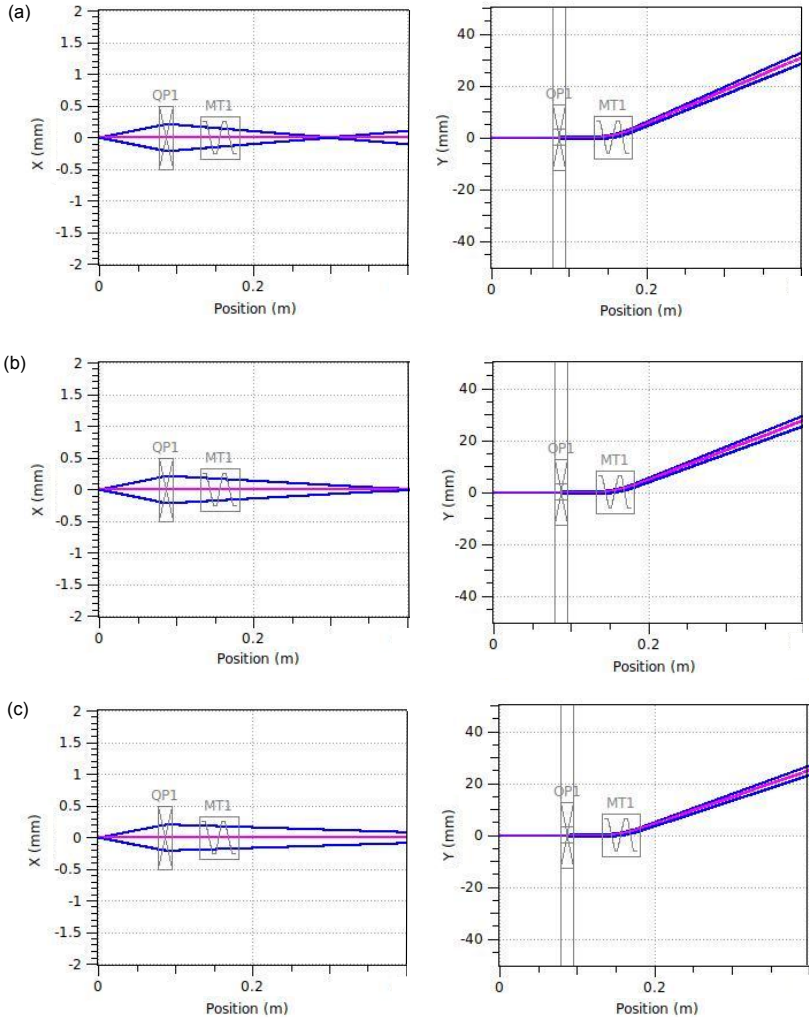

Figure 3.9: Beam envelopes for electron beams with divergence angle of 5 mrad. The system consists of a quadrupole magnet (∇B=275 T/m and B_{dipole}=0.7 T) which is focusing in the x-direction and a dipole magnet that bends the path of the beam in the y-direction. Envelope for **(a)** 80 MeV, **(b)** 90 MeV, **(c)** 100 MeV.

Note that the positions of the quadrupole and of the dipole in figure 3.9 remain unchanged and it is only the energy of the electron beam that is different between the different envelopes. This illustrates the energy depen-

dence of the focal length of magnetic quadrupole lenses, see equation 2.1. In the y-direction it is visible how the change in the direction of motion is smaller for electrons with higher energy, when they pass through the dipole magnet. The positions of the quadrupole lens and the dipole magnet correspond to the ones used in the experiments, discussed in section 3.5, but the magnetic field gradient is higher than in the actual experiments.

3.5 Results and Analysis

Using the experimental setup described in section 3.1, a typical energy spectrum taken with a quadrupole lens is displayed in figure 3.10.

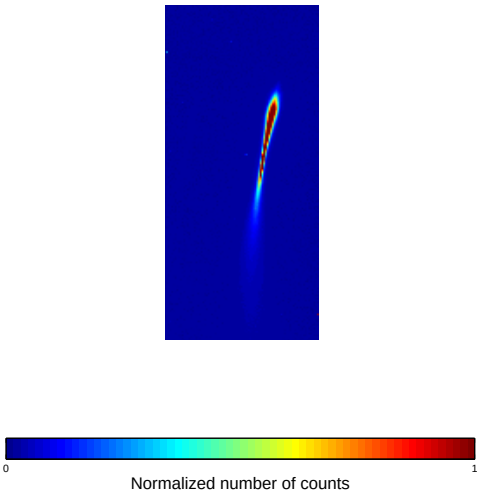

Figure 3.10: An energy spectrum taken with 19.1 mm quadrupole lens positioned 58 mm away from the gas jet.

The waist of the energy spectra is 0.9 mm wide on the screen and at its "head" it is 2 mm wide.

The first result that would need to be verified is that the quadrupole lens actually focuses electron beams. In figure 3.11 a comparison of spectra taken with and without a quadrupole lens under the same conditions can be made. Each of the images consists of 10 averaged spectra, without any special selection being made. The front edge of the quadrupole is placed 58 mm from the gas jet, the gas used is hydrogen and the backing pressure is 13 bar. It is easy to conclude that the spectra with the quadrupole is considerably thinner (1 mm at the waist) than the one without ($\sim$8 mm). This means that also electrons of energies that are not focused on the screen are less divergent, than without the quadrupole lens.

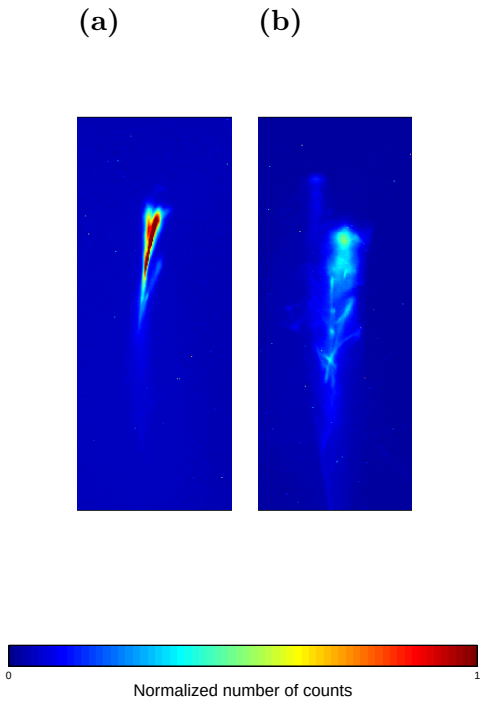

Figure 3.11: **(a)** Averaged energy spectra with 19.1 mm long quadrupole magnet. **(b)** Averaged energy spectra without quadrupole magnet. For both spectra the gas used was hydrogen and the backing pressure was 13 bar.

The next, and perhaps most important, thing to investigate from the experiments is how the waist of the spectrum moves vertically when the position of the quadrupole magnet is altered. The tendency in figure 3.12 is that the waist moves towards higher energies when the distance between the gas jet and the quadrupole lens increases. This is in agreement with the simulated spectra. Another conclusion that can be drawn from figure 3.12 is that the angle of inclination for the spectra increases as the quadrupole lens is moved further away. This could indicate that the quadrupole magnet is slightly misaligned with respect to the electron beam and that the center of the beam passes through the quadrupole lens further and further away from the center of the lens.

As can be seen in figure 3.12 the waist becomes harder to locate when the quadrupole lens is moved further away from the electron source. Reasons for this could be that the energy focused by the quadrupole lens is higher than any energy in the electron beam or the fact that the spatial separation on the screen between different energies becomes smaller and smaller for higher energies. The positions on the screen corresponding to 90 and 100 MeV are only 3 mm apart. Therefore only the three first positions (58 mm,

68 mm and 78 mm from the gas jet) for the quadrupole lens have been evaluated. The method used to evaluate the spectra was to summarize all the images taken at each of the positions for the quadrupole. In this way the influence on the results from shot to shot fluctuations are minimized.

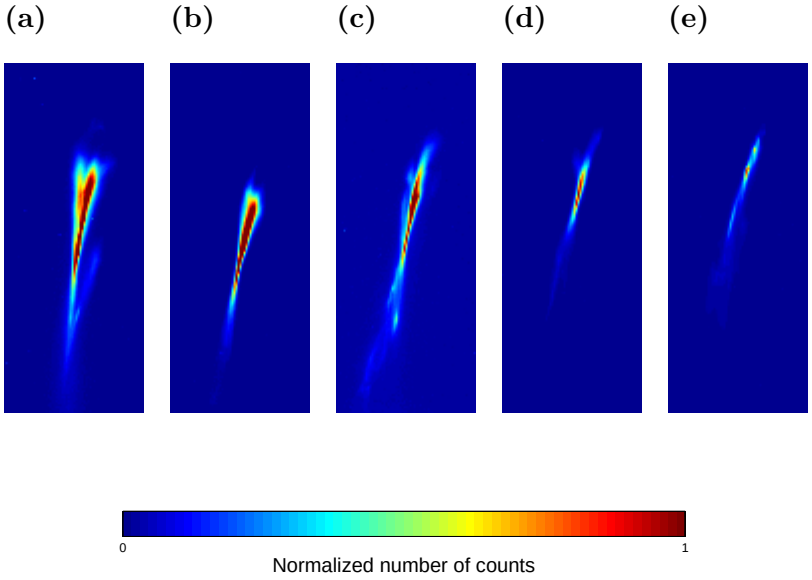

Figure 3.12: Energy spectra taken with different distances from the gas jet to the 19.1 mm long quadrupole lens. For all spectra the gas used was hydrogen and the backing pressure was 13 bar. Each spectrum is the sum of 8 to 10 images taken at each position for the quadrupole magnet. Distance from source to quadrupole: **(a)** 58 mm **(b)** 68 mm **(c)** 78 mm **(d)** 88 mm **(e)** 98 mm

From figure 3.12 the position of the waist of the energy spectra is estimated within an interval and then the corresponding energy is calculated, see appdendix A for details. The dipole magnet is assumed to produce a completely homogeneous magnetic field of 0.7 T without any fringe fields. In table 3.1 the results from these calculations are presented together with values calculated with equation 2.1 and the lens formula.

$$\frac{1}{f} = \frac{1}{a} + \frac{1}{b} \tag{3.5}$$

f is the focal length of the quadrupole lens and a and b are defined as seen in figure 3.13

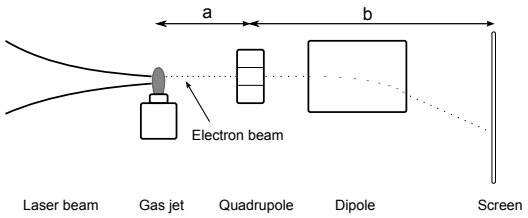

Figure 3.13: The distances a and b from the lens formula marked in the setup.

It should be noted that, depending on the Larmor radius, the electrons will actually travel longer than the distance b. However, for the setup used in these experiments the difference is only a few millimetres and the discrepancy for the calculated energies in table 3.1 is less than 1%.

Drift	Experimental Value	Calculated Value, ∇B=175 T/m, ω=19.1 mm	Calculated Value, ∇B=175 T/m, ω_{eff}=17.1 mm
58 mm	55±2 MeV	52 MeV	48 MeV
68 mm	63±2 MeV	58 MeV	52 MeV
78 mm	68±2 MeV	64 MeV	57 MeV

Table 3.1: Focused energy on the screen by the 19.1 mm long quadrupole lens. Drift denotes the distance from the gas jet to the quadrupole.

The results displayed in Table 3.1 where the physical length of the quadrupole length has been used in the calculations, show better agreement than the ones calculated with the effective length. A reason for this could be that the assumption that the quadrupole lenses of different physical length would have similar fringe fields was wrong. The fringe field for the 19.1 mm long quadrupole lens was never measured. A further reason could be that the fringe field was measured close to the edges of the opening in the 25.4 mm quadrupole lens, see figure 2.10. The fringe field closer to the optical axis might be different and that is where the electrons passed in the experiment.

The experimental values are similar to the calculated values, nevertheless there are many factors that might have influenced the results. One of them is the approximation of the dipole magnet with a completely homogeneous dipole field. This will cause an uncertainty when calculating the corresponding energy to a certain position in the spectra. Another problem is that the energy spectra were not sufficiently broad and thereby it was difficult to pinpoint the location of the waist.

Chapter 4

Conclusions and Outlook

4.1 Conclusion

The aim of this master thesis project was to design, produce and characterize a set of magnetic quadrupole lenses. The main goals with the characterization were to determine the magnetic field inside the lenses and to decide their focal lengths for different energies.

Simulations of the magnetic field inside quadrupole lenses were carried out in order to determine an appropriate design. These simulations were however limited, as they were only performed in two dimensions and did thus not take any fringe fields into consideration. This might be the cause for the non-coherence between the simulated and the actual gradient. As the magnetic field on the surface of the NdFeB-magnets is very close to the simulated values, it is likely that there is room for improvements in the mounting of the NdFeB-magnets in the yokes. When using the quadrupole lenses in the future it would be advisable to polish the inside of the yokes first, to make a larger contact surface between the yoke and the NdFeB-magnets. If it is possible to increase the gradient of the magnetic field in the quadrupole lenses, it would be easier to focus or guide electrons of higher energies. It would also help to maintain the short pulse duration of the electron beam.

The dipole magnet used to separate electrons of different energies in the experiments is well functioning for electrons of lower energies whereas it would be necessary to use a longer or stronger dipole for high energy electrons. Otherwise the energy separation is to small to distinguish with high precision.

The aims of this master thesis project have been fulfilled in terms of design, production and characterization of the miniature magnetic quadrupole lenses and the results from the experiments confirm that the quadrupole lenses can focus electron beams from a laser-plasma accelerator.

4.2 Outlook

There are many ways to further develop and expand this project, the most obvious one is to try more than one quadrupole lens at the time in the laser-plasma accelerator. If two lenses were used the electron beam could be focused simultaneously in both the horizontal and vertical direction. Hence it would be possible to produce energy spectra that would be both narrow and have an improved energy resolution. The complexity of the setup would clearly increase with the number of quadrupole lenses used, therefore it might be necessary to improve the mounts for the quadrupoles so that their alignment could be finely tuned.

Another area of interest is to enable transport of the electron beam over longer distances and thereby widen the range of possible applications. The ideal situation would be to completely eliminate the beam divergence and to produce a parallel beam, though this is only possible to accomplish for completely monoenergetic electron beams. Quadrupole lenses could however strongly reduce the divergence of the electron beam and thus prolong the distance over which the beam could be transported.

To preserve the short pulse duration of the electron beam it is vitally important to use quadrupole lenses with as high gradient of the magnetic field as possible. One way of increasing the gradient would be to use a Halbach design for the quadrupole lenses. In short, this is an array of magnets positioned in a circle in such a way that the components of the magnetic field from the different magnets completely cancels out on the outside of the circle and add together on the inside, see figure 4.1.

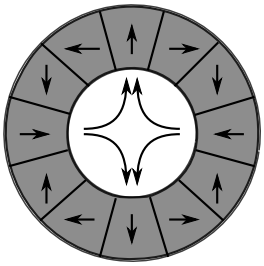

Figure 4.1: A Halbach design for a magnetic quadrupole lens. The magnets are grey and the arrows indicate the direction of the magnetic field.

Not only can the quadrupole lenses in themselves and their use be improved, but it is also important to remember that the quadrupole lenses will only be working for one energy at the time and thus a stable monoenergetic electron beam would greatly enhance the functionality of the quadrupole lenses.

In the rapidly expanding field of laser-plasma accelerated electrons there are numerous improvements to be made and the development of well-functioning magnetic quadrupole lenses will enable further progress.

Appendix A

Dipole

The aim of these calculations is to determine the vertical displacement, from a homogeneous magnetic dipole field, of electrons with specified energy and angle of incidence. The radius of curvature for the electrons inside the dipole field is determined by equation 3.1, which is repeated here:

$$R = \frac{p}{|q|B}$$

a, b, $\hat{x}$ and θ are defined according to figure A.1 and y and x are the vertical and horizontal position of the electron respectively. The vertical displacement, d, is considered to be the difference in the y-coordinate from where the electron enters the dipole and after a specified distance, in this case where it hits the screen. The origin has the position marked in figure A.1.

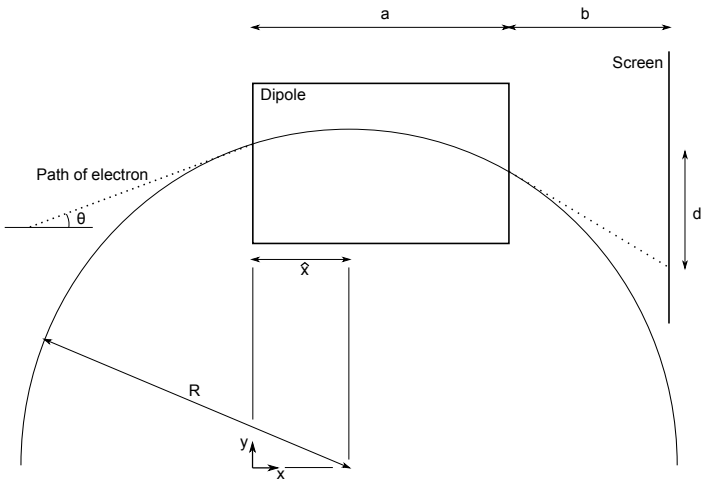

Figure A.1: The path of an electron beam passing through the dipole

Inside the dipole the position of the electron can be described by the equation of a circle.

$$(x - \hat{x})^2 + y^2 = R^2 \tag{A.1}$$

Then y can be expressed as a function of x inside the dipole.

$$y(x) = \sqrt{R^2 - (x - \hat{x})^2} \tag{A.2}$$

The direction of motion of the electron inside the dipole can also be determined as the derivative of y.

$$y\prime(x) = \frac{x - \hat{x}}{\sqrt{R^2 - (x - \hat{x})^2}} \tag{A.3}$$

To calculate $\hat{x}$ it can be noted that at the left boundary of the dipole magnet the derivative of y and $\tan\theta$ must be equal. This condition can be used to derive $\hat{x}$ in the following way:

$$y\prime(0) = \frac{-\hat{x}}{\sqrt{R^2 - (-\hat{x})^2}} = \tan\theta$$

$$\Longleftrightarrow$$

$$\hat{x}^2 = \tan^2\theta\left(R^2 - \hat{x}^2\right)$$

$$\Longleftrightarrow$$

$$\hat{x} = \frac{R\tan\theta}{\sqrt{1 + \tan^2\theta}} \tag{A.4}$$

Using equations A.2, A.3 and A.4, d can be expressed as a function of a, b, R and θ.

$$d = y(0) - y(a) + by\prime(a) =$$

$$\sqrt{R^2 - \hat{x}^2} - \sqrt{R^2 - (a - \hat{x})^2} + b\frac{a - \hat{x}}{\sqrt{R^2 - (a - \hat{x})^2}}, \tag{A.5}$$

$$\text{where } \hat{x} = \frac{R\tan\theta}{\sqrt{1 + \tan^2\theta}}$$

Bibliography

[1] T. Tajima, J.M. Dawson, "Laser electron accelerator", *The American Physical Society*, vol. 43, p. 267-270, 1979

[2] S. P. D. Mangles, C. D. Murphy, Z. Najmudin, A. G. R. Thomas, J. L. Collier, A. E. Dangor, E. J. Divali, P. S. Foster, J. G. Gallacher, C. J. Hooker, D. A. Jaroszynski, A. J. Langley, W. B. Mori, P. A. Norrey, F. S. Tsung, R. Viskup, B. R. Walton and K. Krushelnick, "Monoenergetic beams of relativistic electrons from intense laser-plasma interactions" *Nature*, vol. 431, p. 535-538, 2004

[3] C. G. R. Geddes, Cs. Toth, J. van Tilborg, E. Esarey, C.B. Schroeder, D. Bruwiler, C. Nieter, J. Cary and W. P. Leemans, "High quality electron beams from a laser wakefield accelerator using plasma-channel guiding", *Nature*, vol. 431, p. 538-541, 2004

[4] J. Faure, Y. Glinec, A. Pukhov, S. Kiselev, S. Gordienko, E.Lefebvre, J.-P. Rousseau, F. Burgy and V. Malka, "A laser-plasma accelerator producing monoenergetic electron beams", *Nature*, vol. 431, p. 541-544, 2004

[5] W. L. Kruer, *The physics of laser plasma interaction*, Chapter 6, Westview Press, Oxford, United Kingdom, 2003

[6] T. Katsouleas, "Electrons hang ten on laser wake", *Nature*, vol. 431, p. 515-516, 2004

[7] O. Lundh, *Laser-driven beams of fast ions, relativistic electrons and coherent X-ray photons*, PhD thesis, Department of Physics, Faculty of engineering, Lund University, 2008

[8] V. Malka, J. Faure, Y. A. Gauduel, E. Lefebvre, A. Rousse and K. T. Phouc, "Principles and applications of compact laser-plasma accelerators", *Nature Physics*, vol. 4, p. 447-453, 2008

[9] J. K. Lim, P. Frigola, G. Travish, J. B. Rosenzweig, S. G. Andersson, W. J. Brown, J. S. Jacob, C. L. Robbins and A. M. Tremain, "Adjustable, short focal length permanent-magnet quadrupole based electron beam

final focus system", *Physical Review Special Topics - Accelerators and Beams*, vol. 8, p. 072401 1-17, 2005

[10] T. Eichner, F. Grüner, S. Becker, M. Fuchs, D. Habs, R. Weingertner, U. Schramm, H. Backe, P. Kunz and W. Lauth, "Miniature magnetic devices for laser-based, table-top free-electron lasers", *Physical Review Special Topics - Accelerators and Beams*, vol. 10, p. 082401 1-9, 2007

[11] R. Weingartner, M. Fuchs, A. Popp, S. Raith, S. Becker, S. Chou, M. Heigoldt, K. Khrennikov, J. Wenz, T. Seggebrock, B. Zeitler, Zs. Major, J. Osterhoff, F. Krausz, S. Karsch and F. Grüner, "Imaging laser-wakefield-accelerated electrons using miniature magnetic quadrupole lenses", *Physical Review Special Topics - Accelerators and Beams*, vol. 14, p. 052801 1-7, 2011

[12] H. Wollnik, *Optics of Charged Particles*, Chapter 3, Academic Press, Inc., Orlando, USA, 1987

[13] H. H. Rose, *Geometrical Charged-Particle Optics*, Chapter 4, Springer Verlag, Berlin-Heidelberg, Germany, 2009

[14] Z. Segalov, "Ion optics of displaced quadrupole lens charge selector", *Nuclear instruments and methods*, vol. 130, p. 607-609, 1975

[15] B. E. A. Saleh, M. C. Teich, *Fundamentals of Photonics*, Chapter 1, John Wiley and Sons, Inc., Hoboken, USA, 2007